Solar Energy Materials & Solar Cells 252 (2023) 112203

Contents lists available at ScienceDirect

Solar Energy Materials and Solar Cells

journal homepage: www.elsevier.com/locate/solmat

Thermo-optical performance of bare laser-synthesized TiN nanofluids for direct absorption solar collector applications

Sajid Farooq [a,b], Caio V.P. Vital [c], Gleb Tikhonowski [d], Anton A. Popov [d], Sergey M. Klimentov [d], Luis A.G. Malagon [a], Renato E. de Araujo [c], Andrei V. Kabashin [e,*], Diego Rativa [a,f]

[a] Institute of Innovation and Technology, University of Pernambuco, Recife, Brazil
[b] Center for Lasers and Applications, Instituto de Pesquisas Energéticas e Nucleares, Av. Prof. Lineu Prestes 2242, São Paulo, 05508-000, Brazil
[c] Department of Electronics and Systems, Federal University of Pernambuco, Recife, Brazil
[d] Bionanophotonic Lab, Institute of Engineering Physics for Biomedicine PhysBio, National Nuclear Research University MEPHI, Moscow, 115409, Russia
[e] Aix Marseille Univ, CNRS, LP3, Campus de Luminy, Case 917, 13288, Marseille, France
[f] Applied Physics Program, Federal Rural University of Pernambuco, Recife, Brazil

ARTICLE INFO

Keywords:
Nanofluid
Titanium nitride (TiN)
Plasmonics
Solar energy
Pulsed laser ablation in liquids

ABSTRACT

Titanium nitride (TiN) nanoparticles (NPs) look very promising for solar energy harvesting owing to a strong plasmonic absorption with the maximum in the near-infrared range. However, the synthesis of TiN nanofluids is very challenging as one has to combine the plasmonic feature and long-term colloidal stability to withstand harsh conditions of direct absorption solar collectors (DASC). Here, we explore solutions of bare (ligand free) TiN NPs synthesized by pulsed laser ablation in acetone as the nanofluid. We show that such NPs are low size-dispersed (mean size 25 nm) and exhibit a broad absorption peak around 700 nm, while their negative charge ensures a prolonged electrostatic stabilization of solutions. Solar weighted absorption coefficient of such TiN nanofluids reaches 95.7% at very low volume fractions (1.0×10^{-5}), while nanofluid temperature can be increased up to 29 °C under 1.25-sun illumination. Our data evidence that the thermal efficiency of a DASC using TiN nanofluid is 80% higher compared to Au-based counterparts. The recorded high photothermal efficiency and excellent colloidal stability of TiN nanofluids promises a major advancement of DASC technology, while laser-ablative synthesis can offer easy scalability and relative cost-efficiency required for the implementation of systems for solar energy harvesting.

1. Introduction

The increasing energy demands of modern industrial society puts into forefront solar energy as a clean, renewable and virtually infinite energy resource [1,2]. Being exploited via photovoltaic or photothermal energy conversion mechanisms, solar energy can be used in a plethora of applications, including desalination [3], electricity generation [4], space-heating, and domestic hot-water provision [4,5]. Direct absorption solar collectors (DASC) employing liquid absorbing media present one of the simplest geometries for solar energy exploitation [6]. Since most widely-available DASC working fluids (water, ethylene glycol, and oil) have relatively weak absorption, nanoparticles (NPs) with a broad absorption band in solar emission spectrum [7–11] are typically added to the solar collector base fluid. Such mixtures, termed nanofluids, can be formed by exploring NPs of different types of materials, including dielectrics [12], semiconductors [13,14], pure metals [15,16], doped metals [17–20], metal oxides [21–23], metal nitrides [24], in order to improve thermophysical properties of base fluids. In particular, Chen et al. showed that solar thermal conversion efficiency can be increased by up to 95% by adding carbon multi-walled nanotubes (0.02 wt%) into a base fluid [25], while the addition of graphene oxide/Ag NPs to water leads to the increase of DASC efficiency by 91.6% [26]. Wang et al. studied composite ZnO–Au oil-base nanofluid that exhibited 240% thermal conversion enhancement of the DASC, as compared with the pure base fluid [27]. It was also demonstrated that thermal efficiency can be enhanced by 28.3% at the volume fraction of 0.2 wt%, by employing Al_2O_3 nanofluids [28]. Although these nanofluids show superior opto-thermal properties, their application prospects have been limited so far due to series of challenges, including low dispersion stability, material cost and complex synthesis procedures of nanoparticles [29–31]. Plasmonic noble metal NPs occupy a particularly important

* Corresponding author.
E-mail address: andrei.kabashin@univ-amu.fr (A.V. Kabashin).

https://doi.org/10.1016/j.solmat.2023.112203
Received 25 November 2022; Received in revised form 7 January 2023; Accepted 14 January 2023
Available online 20 January 2023

Nomenclature

Greek Symbol

η	Thermal efficiency
λ	Wavelength
ρ	Density
σ	Cross-section

Abbreviations

a	Radius
Am	solar weighted absorption coefficient
AM 1.5	Direct solar radiation at air mass 1.5
ASTM	American Society for Test-ing and Materials
fs	Femtosecond
$\dot{m}$	Mass flux
Au	Gold
c	Speed of light in a vacuum
c_p	Specific heat
DASC	Direct absorption solar col-lectors
G_T	Solar incident flux
h	Collector height
^{h}conv	Convective heat transfer
^{I}rad	Incident solar intensity
kV	Kilowatt
L	Length
n	Refractive index
NP	Nanoparticle
p	Volume fraction
PLAL	Pulsed laser ablation in liq-uids
T	Temperature
TiN	Titanium nitride
U_x	Flux velocity
UV	Ultra-violet
V	Volume

niche related to nanofluid-based DASC technology [32–34]. Capable of supporting oscillations of free electrons (plasmons), these NPs exhibit strong resonant absorption in the visible spectrum due to the generation of Localized Plasmon Resonances (LPR). As an example, Au NPs in size range of 30–60 nm exhibit a molar absorption coefficient of ~ $7.66 \times 10^9 M^{-1} cm^{-1}$, which is four or five orders of magnitude higher than that of conventional absorbing dyes such as indocyanine green ($1.08 \times 10^4 M^{-1} cm^{-1}$), rhodamine-6G ($1.15 \times 10^5 M^{-1} cm^{-1}$) and malachite green ($1.49 \times 10^5 M^{-1} cm^{-1}$) [35]. Due to so high optical absorption, noble metal NPs look very promising constituents for solar energy harvesting applications. In particular, it was found that the presence of Ag NPs in base-fluid (H_2O) provides 144% photothermal conversion efficiency under the sun illumination [36], while the addition of Au NPs to water can improve the photo-thermal conversion efficiency by up to 21%, as compared to the base fluid [37]. As reported by Taygi et al., Al nanofluid exhibited up to 10% higher efficiency of DASC compared to flat plate collectors [10]. Owing to excellent chemical stability and high optical absorption, Au NPs look as excellent candidates for nanofluid implementations, but having plasmonic peak around 520–560 nm, therefore, they cannot absorb light in the near-infrared range of solar spectrum limiting their application prospects [35]. The absorption range of Au-based nanomaterials can be extended to near-infrared by designing complex nano-architectures such as nanorods [33,38] or core-shells [20], but these structures are typically costly and require more complicated capping to be stabilized in solutions.

The employment of alternative plasmonic nanomaterials such as transient nitride NPs is another possible solution to this spectral mismatch problem. Here, titanium nitride (TiN) NPs look especially promising due to a broad red-shifted plasmonic-related absorption peak compared to other plasmonic counterparts (Ag, Au, Cu, etc.) [39,40]. Indeed, several recent studies reported the improvement of nanofluid performance by employing TiN and Au–TiN alloy NPs [41–43]. However, the elaboration of TiN nanofluids for solar energy harvesting is still not free of challenges. One of problems consists in the lack of methods for low-cost, scalable fabrication of stable colloidal NPs solutions, which could preserve their long-term properties under light-induced heating. Indeed, nanomaterials prepared by wet chemical methods [44,45] have nearly zero zeta potential and require organic protective ligands or surfactants to avoid agglomeration and precipitation effects. However, such a capping can stabilize colloidal solutions only for a limited time span ranging from several weeks to several months. In contrast, suspensions of NPs prepared by dry fabrication pathways such as plasma synthesis are typically composed of broadly size dispersed NPs and aggregates [46–49], which is not consistent with long-term stability requirements. Furthermore, solar harvesting applications imply a drastic increase of nanofluid temperature under light-induced heating, which can alter the properties of NPs conjugates and destabilize the solution.

We believe that the above-stated problems in the synthesis and applications of TiN nanofluids can be resolved by the employment of bare (ligand-free) colloidal nanomaterials prepared by methods of pulsed laser ablation in liquids (PLAL) [50–54]. The PLAL technique is based on laser-induced ablation from a solid-target immersed in a liquid ambient (deionized water, acetone, ethanol, etc.) to produce nanoclusters, which then cool down and coalesce to form a colloidal NPs solution. As we showed previously, femtosecond (fs) laser ablation from a target [52] or colloidal solutions [53] is especially efficient to control size characteristics of formed NPs. A high-efficiency in fabrication of a variety of nanomaterials and exceptional cleanness of synthesis procedure made PLAL very popular for last decade promising attractive applications in biomedicine [55–57], photovoltaics [58], catalysis [59,60], etc. One of the unique properties of PLAL consists in the possibility of obtaining extremely stable NPs solutions in the absence of ligands [52–54]. Such a stability is due to a strong electric charge of laser-synthesized NPs, which makes possible an electrostatic stabilization of solutions via electric repulsion of NPs [60]. As an example, colloidal solutions of bare Au and TiN NPs prepared by laser ablation in deionized water typically have negative zeta potential with an absolute value higher than 30–35 mV, which makes the solutions stable for many years even during their storage at room temperature [52–54]. In addition, laser-ablative approach becomes much less costly than chemical synthesis techniques under industrial production scale when the productivity values are higher 550 mg/h[61]. It is worth also noting that TiN is a highly abundant and very cheap material with the 1000-fold lower cost compared to Au.

We suppose that high stability in the absence of ligands can be one of key factors to achieve long-term performance of nanofluid-based DASC. Anticipating the above-stated advantages, in this paper we explore bare TiN NPs prepared by methods of pulsed laser ablation in liquid ambient as heating elements in solar energy harvesting applications. We show that such bare TiN NPs can indeed much outperform other plasmonic counterparts such as Au NPs.

2. Materials and methods

2.1. Synthesis and characterization of TiN nanofluid

TiN NPs colloids were synthesized by an ultrashort (pulses of 270fs) laser ablation of TiN in acetone at ambient conditions using a procedure

developed by our group [46–48]. Briefly, a hot-pressed TiN target (GoodFellow) was fixed vertically on the wall of a glass vessel filled with analytical grade acetone. A 3 mm diameter beam from a Yb:KGW laser (wavelength 1030 nm, pulse energy 100 μJ, repetition rate 10 kHz) was focused by a 75 mm lens on the surface of the target through a sidewall of the vessel. The ablation vessel was mounted on a platform, which was continuously moved over a 10 × 10 mm section with a velocity of 5 mm/s. The ablation duration was 30 min. After the fabrication, colloidal solutions of TiN NPs were centrifuged (7000 RCF, 5 min, ELMI CM-50 centrifuge) to remove a minor amorphous fraction, which was also formed during the synthesis. The supernatant formed during the centrifugation step was removed, while the residue was dispersed in deionized water and used for the subsequent experiments.

Morphology, size, and composition of the synthesized NPs were characterized by a scanning transmission electron microscopy (STEM) system (acceleration voltage 0.1–30 kV, MAIA 3, Tescan, Czech Republic) coupled with an EDS detector (X-act, Oxford Instruments, UK). The size of the moving objects in a nanofluid was measured by the dynamic light scattering (DLS) using a Zetasizer ZS instrument (Malvern Instruments). The absorption spectrum in the range 400–900 nm has been obtained using a Cary 5000 UV–Vis–NIR spectrophotometer (Agilent).

Colloidal aqueous solutions of spherical Au NPs with a radius of a = 25 nm were obtained commercially from Nanocomposix for a comparative assessment of the photothermal performance. TiN and Au nanofluids had concentrations of 0.05 mg/ml, corresponding to volume fractions of 9.3×10^{-6} and 2.5×10^{-6}, respectively.

2.2. Solar thermal conversion setup

To investigate solar-thermal conversion efficiency of the nanofluids, an artificial sunlight simulator (AM1.5 spectrum, one-to-three suns irradiance, Oriel LCS-100, Newport, USA) was used to irradiate the colloid within a glass cuvette having the length of 1 cm, as shown in Fig. 1. A concave mirror and a lens (both with f = 10 cm) were used to collimate the sunlight at the cuvette. An iris diaphragm was employed to control the illumination area, and a cell/meter (91150V, Newport, USA) was used as a reference to measure the sunlight intensity. The image of the cuvette and its temperature colormap were monitored using a Flir E4 infrared camera, located 20 cm away from the cuvette. The average value of temperature in the section illuminated by the sunlight (1cm × 1 cm) was monitored, with capture rates of two frames per minute.

2.3. Computational models

2.3.1. Single NP

Numerical simulations exploring 3D computational domain and full-wave finite element method (FEM), based on the Radio-Frequency (RF) and Heat Transfer Modules (COMSOL Multiphysics), were employed to calculate absorption and scattering cross-sections spectra of NPs. Two perfectly matched layers (PMLs) with the thickness of 200 nm covered the top and bottom surfaces of the computational domain, minimizing backscattering effects. Finally, perfect electric and magnetic conductor conditions were applied at the sidewall boundaries.

As represented in Fig. 2a, a spherical metallic particle (TiN) with a radius of a = 25 nm is located at the domain origin (0,0,0), surrounded by the base fluid (water, acetone and ethylene-glycol). The particle is shined with a downward-directed plane electromagnetic wave having the polarization plane over the X-axis, described by time-harmonic E-field equations [20,32]. Values of the TiN permittivity were obtained from Ref. [62].

2.3.2. DASC model

As represented in Fig. 2.b, the 2D DASC model considers that the NF flows between two parallels surfaces. The bottom surface (at y = h) is considered as adiabatic, and the top surface (at y = 0) is a transparent glass cover, with area A. In the collector, the flow moves from the inlet (at x = 0) to the outlet (at x = L). In the proposed model, the collector is illuminated with a radiative heat flux given by $q_r = \int I_{rad} d\lambda$, where I_{rad} is the incident solar intensity at the top surface of the collector. The radiation absorbed in the DASC is converted into thermal energy and the heat transfer inside the collector is considered as 2-dimensional steady-state case, which describes the nanofluid temperature distribution, is given by Ref. [10]:

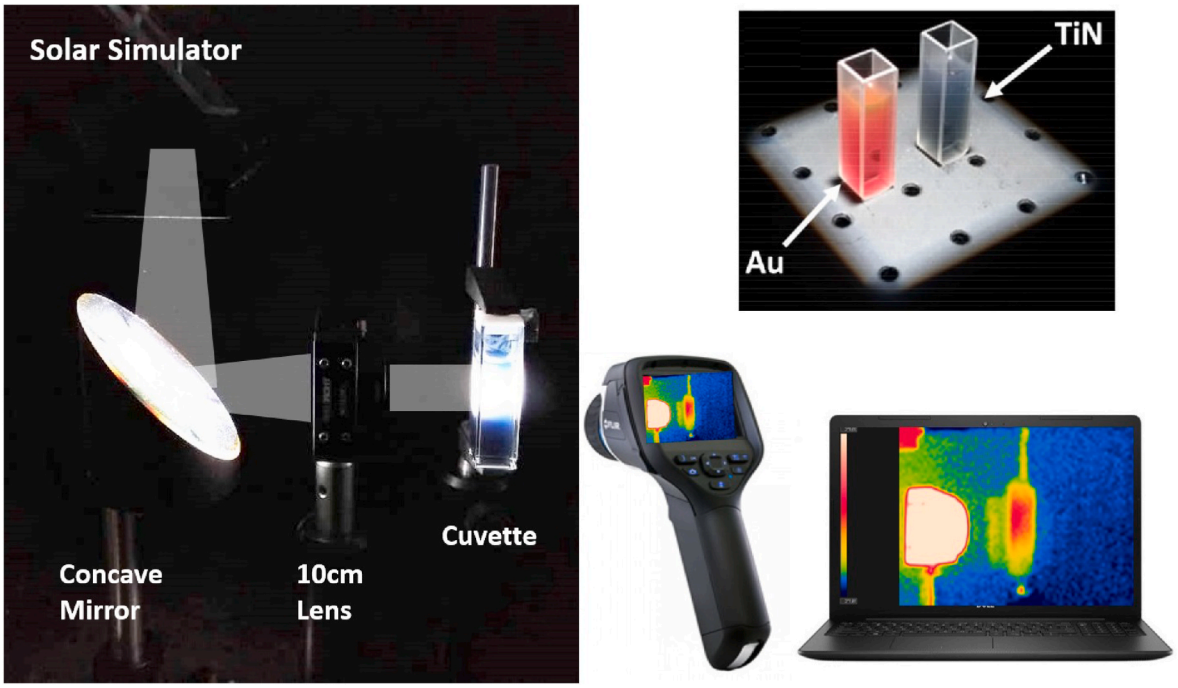

Fig. 1. Schematics of solar thermal conversion experimental setup and photo of cuvettes with colloidal solutions of Au and TiN NPs.

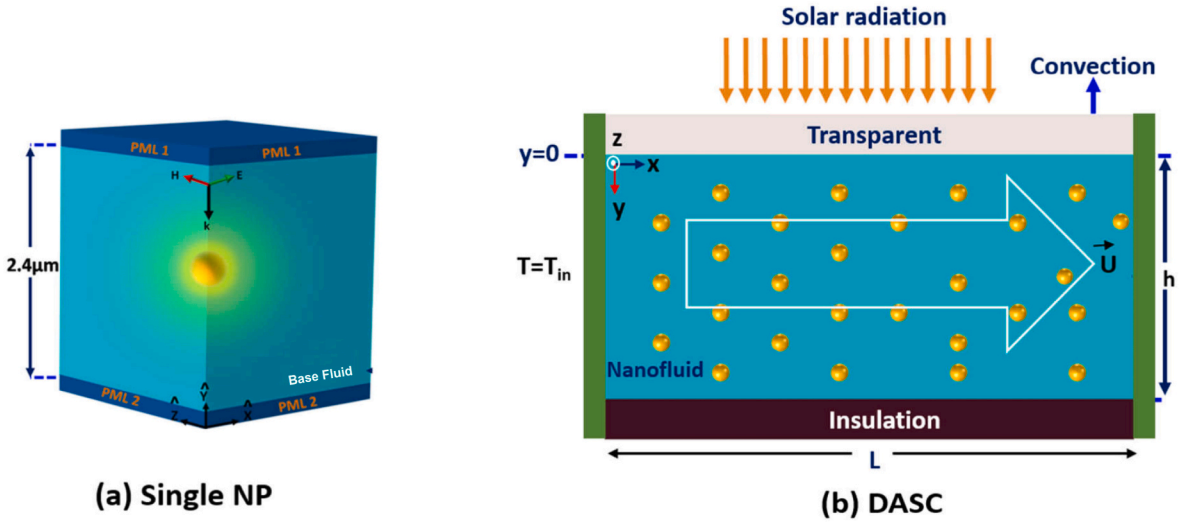

Fig. 2. Computational models: (a) 3D model composed of a metallic NP, an embedding medium (base fluid) and two Perfectly Matched Layers (PML_1 and PML_2); (b) Schematic of the DASC model for thermal and solar harvesting analysis, h and L are thickness and the length of the DASC, respectively. The white arrow indicates the nanofluid flux direction.

$$k_s\frac{\partial^2 T}{\partial y^2}-\frac{\partial q_r}{\partial y}=\rho c_p U_x\frac{\partial T}{\partial x} \tag{1}$$

where U_x is the fluid velocity, ρ and c_p are the density and the specific heat of the working fluid, respectively.

In this model, the DASC has an adiabatic bottom surface, and convection and radiation thermal losses on the top surface are considered. The boundary conditions can be described as:

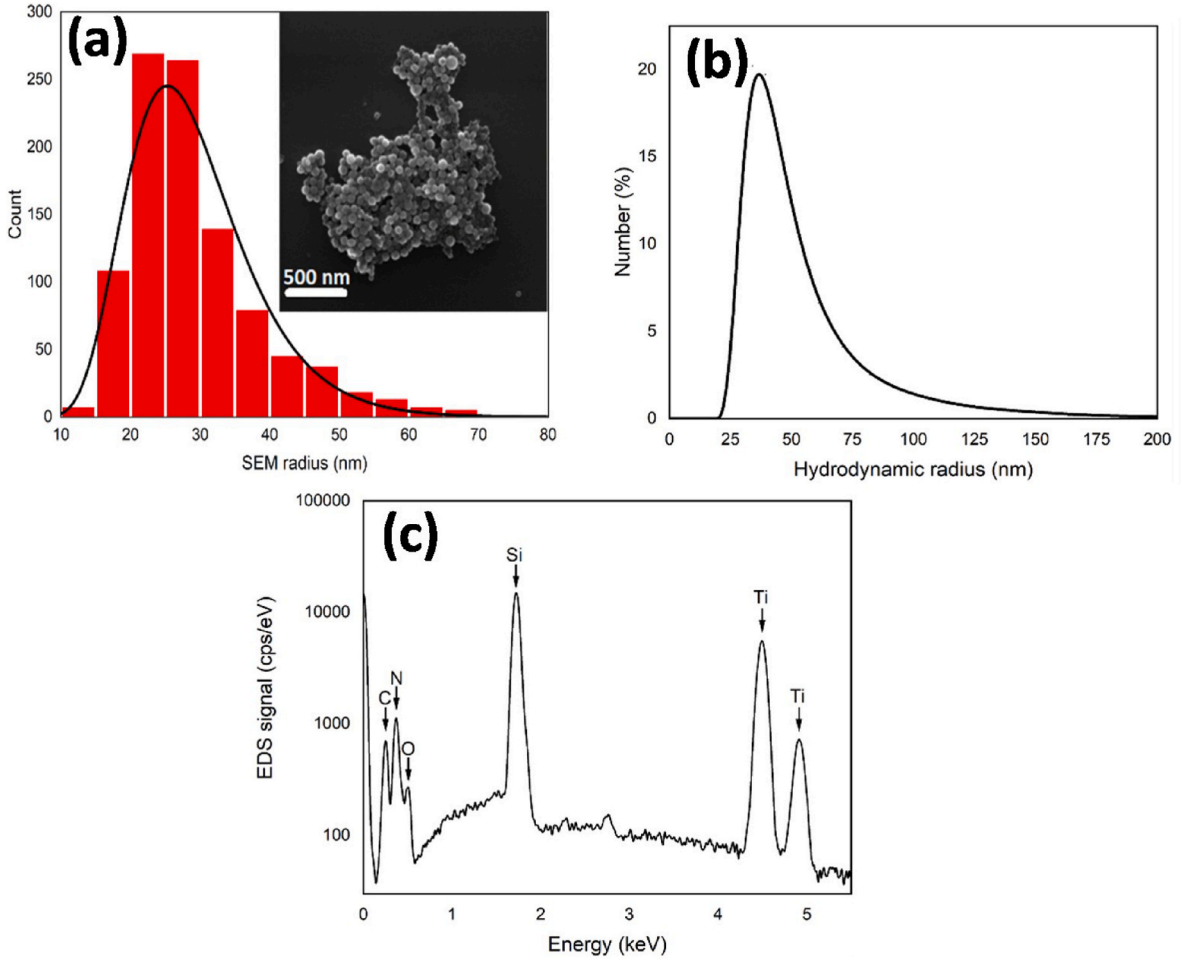

Fig. 3. (a) Size histogram and SEM image (inset) of TiN NPs synthesized by laser ablation in acetone, (b) hydrodynamic size distribution, (c) and energy-dispersive X-ray spectrum of synthesized TiN nanoparticles.

$$k_s \frac{\partial T}{\partial y}\Big|_{y=0} = h_{conv}(T - T_{amb})$$
$$k_s \frac{\partial T}{\partial y}\Big|_{y=h} = 0, \quad (2)$$

where h_{conv} is the convective heat transfer coefficient (10 W/m^{2}K), T_{amb} is the ambient temperature (20 °C).

The DASC thermal efficiency (η) can be calculated as [10]:

$$\eta = \frac{\dot{m} c_{p(\overline{T}_{out} - \overline{T}_{in})}}{A G_T} \quad (3)$$

where $\dot{m}$ is the mass flow of the nanofluid through the collector, G_T is the solar incident flux. Moreover, $\overline{T}_{in}$ and $\overline{T}_{out}$ are the inlet and outlet temperatures, corresponding to the average temperatures at $x = 0$ and $x = L$, respectively.

3. Results and discussions

3.1. TiN nanofluid - experimental evaluation

A typical SEM image and size histogram of the synthesized TiN NPs are shown in Fig. 3.a. One can see that the NPs are mostly spherical, while their size distribution is quite narrow and can be fitted by a log-normal distribution with 25 nm mode size (NP radius), and 15 nm full width at half maximum (FWHM) value.

As shown in Fig. 3.b, the mode value of the hydrodynamic size distribution is almost identical to the mode value of size distribution, measured by the electron microscopy. Therefore, TiN NPs prepared by fs laser ablation indeed move independently in colloidal solutions and do not form aggregates. A qualitative chemical composition of TiN NPs was measured by EDS technique, as shown in Fig. 3.c. The data confirm that the NPs were mainly composed of titanium and nitrogen with minor oxygen fraction. The presence of oxygen can be explained by a natural oxidation of NPs surface. The large silicon (Si) peak in the spectrum is explained by the use of Si wafer as a substrate for the measurement, while the signal from carbon (C) comes from an organic contamination of the measuring vacuum chamber.

The zeta-potential of laser-synthesized TiN NPs was lower than −30 mV, evidencing a large electrostatic charge of laser-synthesized TiN NPs. Therefore, the TiN nanofluids manifest a size uniformity of NPs and the absence of agglomerates. Moreover, we did not observe the formation of any precipitates after the storage of NPs solutions at ambient conditions for more than one year, which is very important for projected solar harvesting applications requiring a high long-term colloidal stability of nanofluids.

3.2. Optical performance of DASC using TiN nanofluids

Fig. 4.a shows the measured absorbance spectrum of dispersed TiN NPs in acetone, which exhibits a broad extinction peak centered at 700 nm with FWHM of 150 nm. One can see in Fig. 4.a the extinctions spectrum, of 25 nm radius TiN NPs, obtained by the numerical simulation. The numerical spectrum shows peak at 700 nm, in accordance with

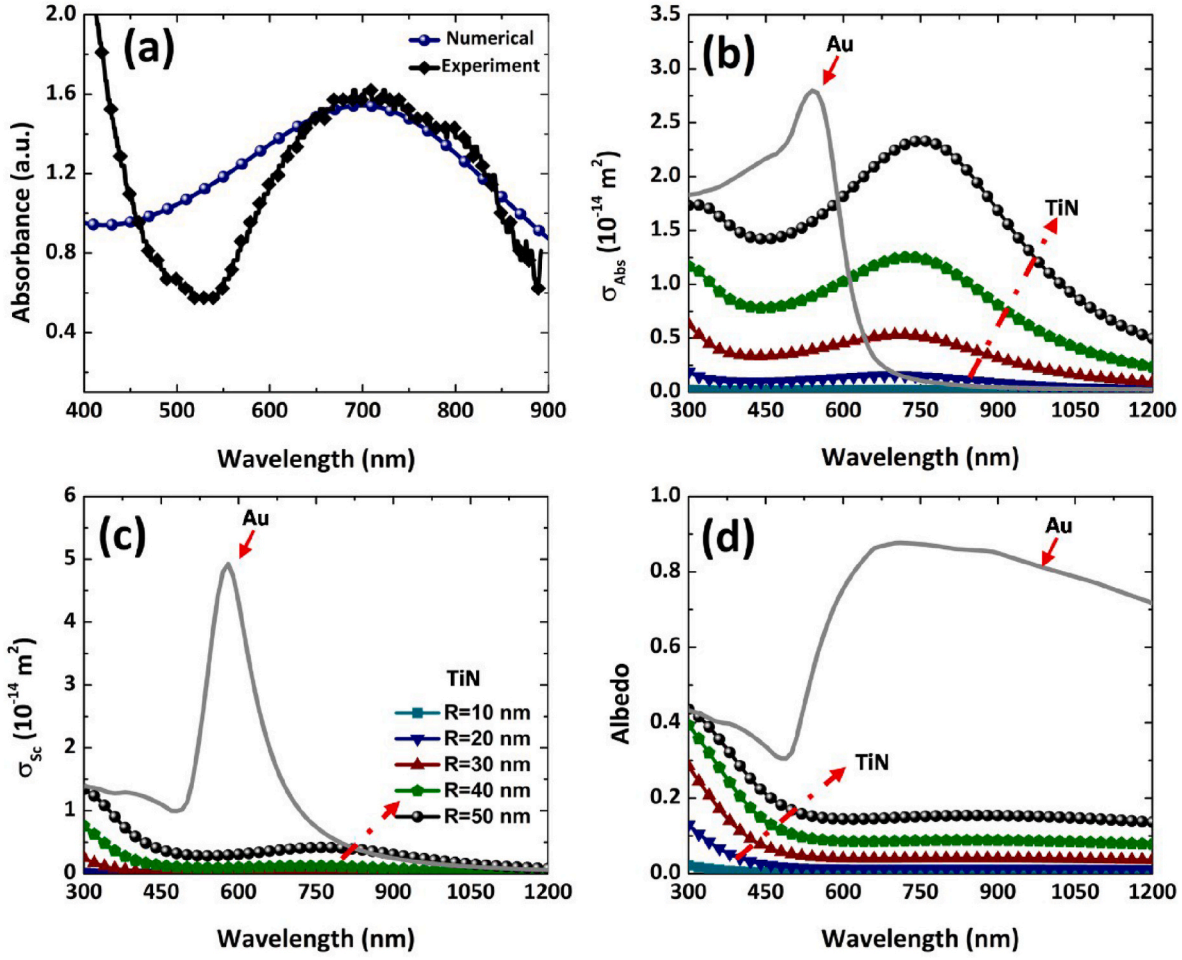

Fig. 4. Spectral dependence of optical properties of TiN NPs: Numerical and experimental absorbance (a), absorption (b) and scattering (c) cross sections; with their respective albedo (d), in aqueous medium. The solid lines present cross-section values of Au NP (a = 25 nm).

the experimental results, validating our numerical model.

Absorptive and scattering properties of a nanostructure rely on its size. Fig. 4.b demonstrates σ_{abs} spectra considering TiN nanospheres with different radius (R = 10, 20, 30, 40 and 50 nm), suggesting that a dipole resonance is the dominant mode for such NPs. Here, the plasmonic peak shifts from 700 to 780 nm, as the particle size increases. Fig. 4.b also shows a spectral dependence for absorption (4) of a Au nanosphere (a = 25 nm). One can see that TiN NP presents a much broader absorption spectrum than Au nanospheres. Moreover, as shown in Fig. 4.c, the scattering-cross section of Au nanospheres is significantly higher than the TiN NP σ_{sca} values. In general, the NPs are efficient for photo-thermal applications if the $\sigma_{sca} < \sigma_{abs}$ condition is satisfied [63, 64].

The albedo factor, or scattering efficiency, defined as $\sigma_{sca}/(\sigma_{abs} + \sigma_{sca})$, can be used to identify efficient nanostructures for thermal applications. As shown in Fig. 4.d, the low albedo values indicate that TiN NPs are mainly absorbing nanostructures, which are efficient for use as working fluids.

The percentage of solar energy absorbed by a TiN nanofluid in a DASC can be estimated by the solar weighted absorption coefficient given by Ref. [65]:

$$A_m = \frac{\int_{300}^{1200} E_\lambda \left(1 - e^{-\alpha h}\right) d\lambda}{\int_{300}^{1200} E_\lambda d\lambda} \tag{4}$$

where E_λ is the spectral distribution of solar intensity (ASTM G173-03 AM1.5 Global). The integration was performed from 300 to 1200 nm. For wavelengths higher than 1200 nm, the contribution of water starts to dominate in optical absorption of any water-based nanofluid. To compare with previous studies, nanofluid concentration is described in terms of the volume fraction given as $p = V_{NPs}/V_{fluid}$, where V_{fluid} is the nanofluid volume, V_{NPs} is the total volume of NPs (i. e. $V_{NPs} = N_{NPs} \times V_{NP}$), N_{NPs} is the number of nanostructures in the working fluid and V_{NP} is the volume of a single particle. Moreover, the nanofluid optical absorption coefficient can be written as $\alpha = (p/V_{NPs}) \times \sigma_{abs}$.

Fig. 5 shows A_m values of working nanofluids in DASC, composed of TiN NP (a = 25 nm) diluted in acetone, water, and ethylene-glycol. The choice of base fluids allows us to explore the TiN nanofluid in three different regimes: water-freezing (0 °C), room (20 °C), and water-boiling (100 °C) temperatures. The height of the DASC is varied from h = 0 to h = 2.5 cm, while volume fractions of TiN ranged between $p = 0$ and $p = 1 \times 10^{-5}$. Relatively small collector height and TiN NP volume fractions ensure optimal absorption efficiencies; for instance, DASC parameters can be selected to obtain A_m values close to 95%, following the solid lines in Fig. 5.

Moreover, as shown in Fig. 5, similar A_m values were found for TiN nanofluids base acetone (n = 1.36) and water (n = 1.33). However, Acetone can be explored in DASC at freezing temperatures (0 °C). Moreover, TiN nanofluid based on ethylene-glycol (n = 1.43) medium can reach higher A_m values with slightly lower NPs concentration. In particular ethylene-glycol based-fluids can be used for applications in temperatures higher than 100 °C.

The use of TiN NPs (1×10^{-5}) inclusions in all three working fluids (water, acetone and ethylene-glycol) leads to A_m values close to ideal absorber conditions for a solar collector with $h = 1$ cm. Solar weighted absorption coefficient was also evaluated for Au water-based nanofluid. For h = 1 cm and Au NP volume fraction close to 1×10^{-5}, the obtained A_m values are not higher than 65%, as shown in Fig. 5.

3.3. Thermal performance of TiN nanofluids

The optical-heating performances of different working fluids were evaluated experimentally. Two nanofluids (Au water-base and TiN Acetone-base), placed in glass cuvette, were illuminated with sunlight, during 25 min. The nanoparticles concentration was adjusted to equalize mass concentrations (0.05 mg/ml) of colloidal suspensions.

As shown in Fig. 6.a, temperature of the TiN nanofluid (in acetone), continuously increases from 20 °C and reaches the maximum at 29 °C after 25 min of 1.25 sun radiation, while Au nanofluid (in water) reaches the maximum temperature at approximately 25 °C under the same conditions. The curves obtained for acetone- and water-based pure fluids

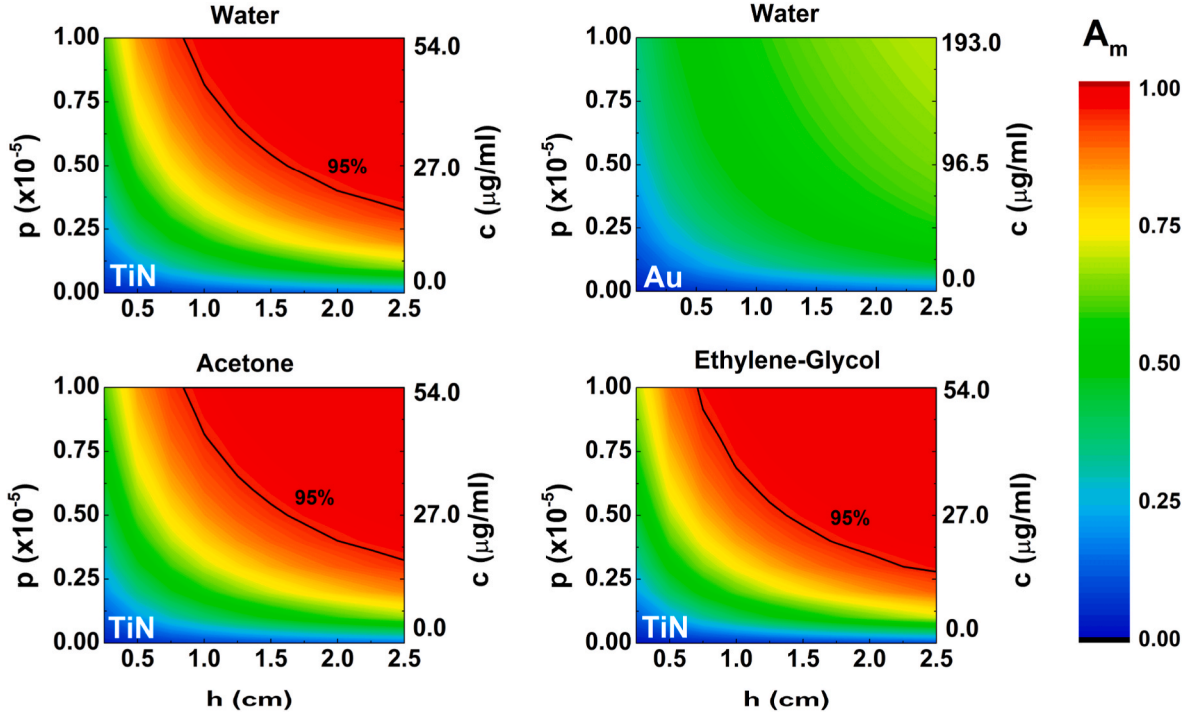

Fig. 5. Solar weighted absorption coefficient for TiN NP (a = 25 nm) immersed in ace-tone, water, and ethylene-glycol: as a function of volume fraction (or mass concentration) and DASC thickness. Au NP in water with same radius are evaluated for comparison. Solid lines indicate the A_m = 95% condition.

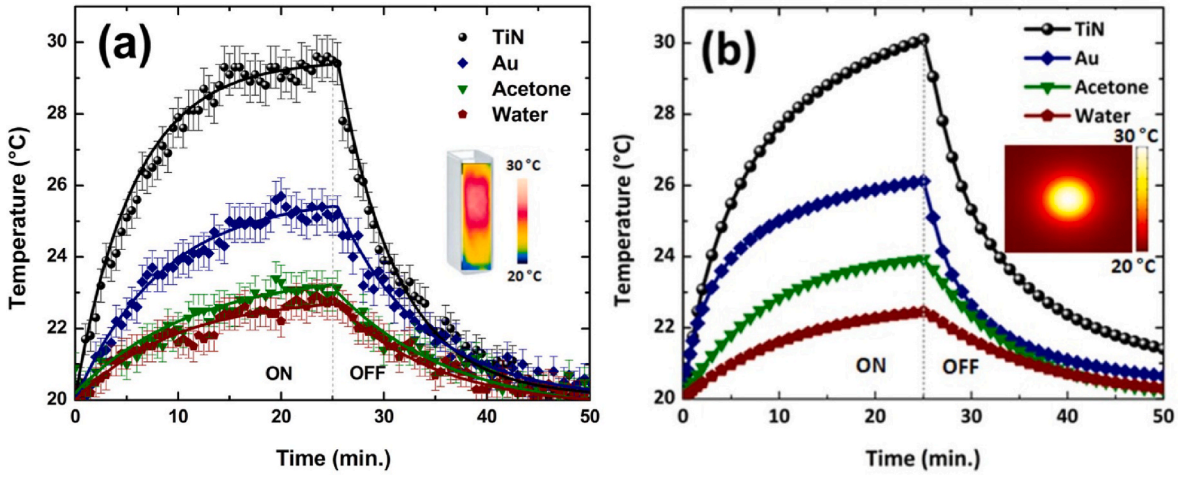

Fig. 6. Time-dependent photo-heating performance of TiN (acetone) nanofluid, Au (wa-ter) base nanofluid, pure acetone and water under 1.25 sun radiation: (a) Experimental results and (b) numerical simulation for a single NP. Vertical gray lines indicate the mo-ment when the illumination is blocked.

(without NPs) are also presented in the figure, showing base-fluid contributions to the heating process. The temperature increase in the nanofluids occurs due to the photothermal conversion by the LPR of the NPs, in which the incident light within the nanofluid absorption spectrum range is absorbed. Moreover, the stagnation of the temperature values after 20 min of exposure is associated with thermal convection losses in system. A better photo-heating performance of the TiN nanofluid can be related to a broader absorption and a lower scattering of the TiN NPs compared to Au counterparts, as commented previously.

Temperature of the optically heated colloid can be estimated by considering the contribution of all the NPs as point-like heat sources [63]. Therefore, the transient heat transfer equation was employed in a 3-dimensional heat conduction model for colloidal solutions of Au and TiN NPs. As can be seen in Fig. 6.b, temperature values obtained with the numerical model are similar to the experimental results, with a similar heating behavior and similar maximal temperatures. After 25 min, the illumination was turned off and the nanofluid temperature started to decrease, due to the thermal losses of the system.

Thermal evaluation was also performed considering a continuous flow ($U_x \neq 0$) of the nanofluid in the DASC. The temperature distribution within DASC was investigated considering different inlet temperatures, corresponding to three typical scenarios: water-freezing (0 °C), room (20 °C), and water-boiling (100 °C) temperatures. The temperature distribution of the TiN acetone-base fluid (with $\overline{T}_{in}$ at 0 °C and 20 °C) and the ethylene-glycol base nanofluid (with $\overline{T}_{in}$ at 100 °C) are shown in Fig. 7. A typical DASC flux velocity ($U_x = 2.0 \times 10^{-3}$ m/s) and 1 Sun incident solar flux ($G_T = 1000$ Wm^{-2}) were considered in the thermal evaluation of the nanofluid.

As can be seen in Fig. 7a and b, when the inlet temperature is equal or smaller than T_{amb} (20 °C), the nanofluid temperature decreases as the distance from the top surface of DASC (where most light energy is absorbed) increases. On the other hand, as shown in Fig. 7c, if the inlet temperature is equal to 100 °C), which is much higher than T_{amb}, the thermal losses become more significant. Therefore, the highest recorded temperatures are in the middle region of DASC. In all three cases, DASC can increase fluid temperature, which illustrates a high potential in TiN NPs based nanofluids at various temperature regimes scenarios.

The thermal efficiency, described by Eq. (3), grows gradually while DASC height is increased. Considering $\overline{T}_{in} = T_{amb} = 20\,°C$, η reaches a value close to 80% in acetone-based nanofluid and up to 90% in water base fluid at h = 1 cm. The maximum efficiency of 92% is recorded for heights larger than 1.5 cm, as shown in Fig. 8.a. The saturation effect, which is characterized by an asymptotic behavior, due to the fact that material absorbs most of the light energy in the light penetration depth, which is about 1.25 cm in case of our nanofluids.

Fig. 8.b depicts the thermal efficiency of DASC as a function of normalized inlet temperature ($\overline{T}_{in} - T_{amb}/G_t$). A decrease in efficiency with the increase in inlet temperature can be related to thermal losses, which are directly proportional to the difference between $\overline{T}_{in}$ and T_{amb}. Analyzing the solar collector thermal behavior under the same operating conditions, one can conclude that DASC using TiN nanofluid exhibits nearly 80% higher efficiency compared to that of spherical Au NPs.

DASCs are known to demonstrate high performance and open up opportunities to explore TiN NPs in different base fluids working in one or another applications or temperature ranges. For comparison purposes, thermal efficiency and A_m coefficients of different nanofluids (reported in the literature) containing only spherical NPs inclusions are shown in Table 1. All solid NPs described in Table 1 can be synthesized by using the PLAL technique.

Our results show that TiN NPs prepared by PLAL exhibit superior properties for DASC applications compared to Au NPs of similar size. The TiN NPs provided a broader absorption band, covering most of the

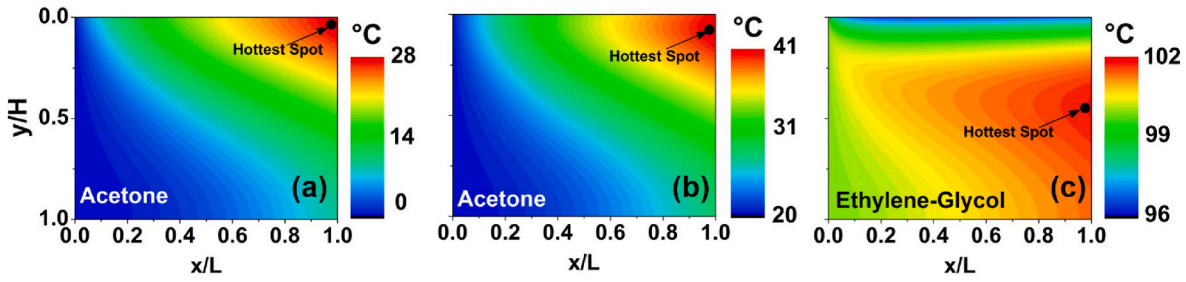

Fig. 7. Temperature distribution within a DASC containing TiN nanofluids, with T_{in} equal to (a) 0 °C and (b) 20°C using acetone base-fluid; and (c) 100 °C using ethylene-glycol base-fluid; with $T_{amb} = 20$ °C and $U_x = 2.0 \times 10^{-3}$ m/s.

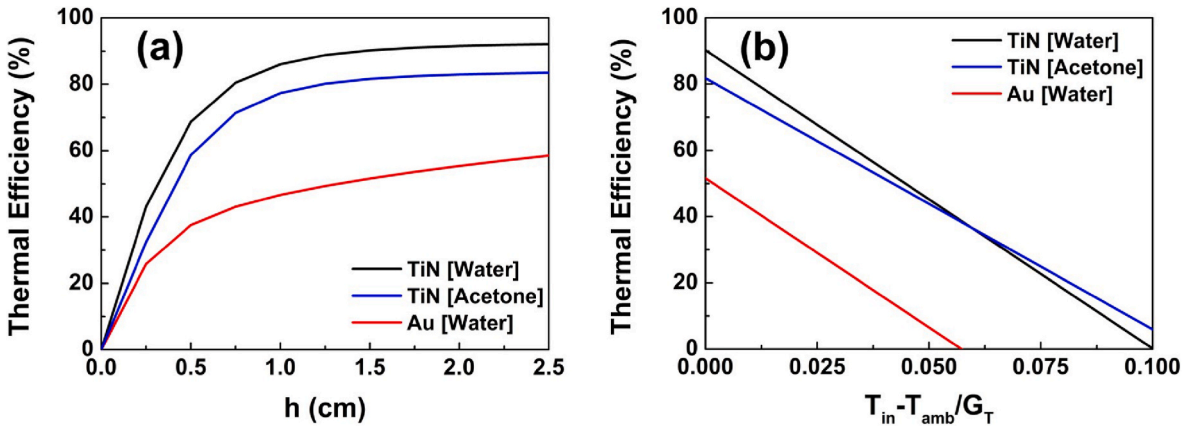

Fig. 8. Thermal efficiency of DASCs using TiN and Au NP at $p = 1 \times 10^{-5}$ as a function of collector height (a) and normalized inlet temperature (b).

Table 1
Solar weighted absorption coefficient of various nanofluids based on spherical shape nanoparticles suspended in base-fluid H_2O and DASC thermal efficiency.

Materials	Structure	Vol. fraction	A_m (%)	h (mm)	Ref.	η (%)
TiN	Solid	1.0×10^{-5}	95.7	10	–	90.2
Au	Solid	5.0×10^{-5}	85.0	10	[65]	51.2
Ag	Solid	2.0×10^{-4}	80.0	10	[66]	40.5
Al	Solid	1.0×10^{-2}	60.0	–	[67]	28.5
SiO_2	Solid	2.0×10^{-4}	20.0	5	[68]	4.8
SiO_2/Ag	Composite	5.0×10^{-5}	69.1	10	[69]	54.4
SiO_2/Au,SiO_2/Ag (blended)	Composite	2.0×10^{-5}	94.2	5	[68]	44.1
TiO_2/Ag	Composite	1.0×10^{-4}	91.0	60	[70]	67.0

solar spectrum (Fig. 4b). Moreover, the photo-assisted thermal efficiency of TiN NPs exhibited better performance than alternative nanofluids based on graphene oxide [26], Al_2O_3 [28], TiO_2 [71], Al [10], carbon nanotubes [25], SiO_2 [68], Au [43] and polystyrene [71].

One of major advantages of nanofluids based on laser-synthesized TiN NPs consists in a very high stability of formed solutions. Indeed, our tests showed that solutions of bare TiN NPs do not present any sign of aggregation or precipitation for several years even under their storage under ambient room temperature conditions.

It is clear that such a stability is due to electrical repulsion effect as laser-synthesized metal NPs have a strong negative charge under nearly identical size and ideally spherical shape [60]. The obtained data on size characteristics of TiN NPs contrast with results of earlier studies, in which aqueous colloidal solutions of bare TiN NPs were prepared by the dilution of commercially available TiN nanopowders [41,46–49]. Indeed, the hydrodynamic size of nanopowder-based TiN NPs measured by DLS was about an order of magnitude larger than the mean size measured by TEM [41,47,49], suggesting a strong aggregation in nanopowder-based suspensions. It is obvious that the presence of such agglomerates is not consistent with long-term stability of nanofluids, as non-uniformity of NPs size distribution typically leads to fast agglomeration and precipitation effects [60]. The stability problem of nanopowder-based nanofluids can somehow be tackled by addition of surfactants or other chemical methods, but such additional step complicates the preparation of a nanofluids and increases its cost, while the efficiency of such stabilization is not very high according to data for chemically synthesized NPs [44,45].

Another potential advantage is related to projected cost-efficiency and easy scalability of laser fabrication process. It is known that PLAL synthesis of plasmonic NPs becomes more economically efficient than wet chemical methods when the productivity rate is higher than 550 mg of NPs mass per hour [61], while even single laser beam-based experimental setups can enable much higher productivity rates up to 4000 mg per hour [72]. Such a productivity rate is equivalent to 80 Lh^{-1} of TiN nanofluid with volume fraction up to 10^{-5}, which is very high. It is also important that the productivity rate can further be increased by using additional laser beams.

4. Conclusion

We synthesized bare (ligand-free) TiN NPs in acetone by using methods of pulsed laser ablation. NPs were low-size dispersed with the mean size of 30 nm, while their strong negative charge (< -30 mV, according to zeta potential measurements) ensured a prolonged electrostatic stabilization of NPs solution in the absence of ligands. Optical spectra from NPs solutions evidenced the presence of a strong and broad absorption band with a maximum around 700 nm associated a dipole plasmon excitation. We also found that TiN NPs are mainly absorbing and have a reduced scattering. A numerical analysis showed that solar weighted absorption efficiency of TiN NPs suspended in acetone fluid was close to 95% at very low volume fractions ($p = 1.0 \times 10^{-5}$), due to broadband absorption, which was much higher than that of Au NPs. The solar thermal experiment demonstrated that TiN nanofluid had two-times temperature increase in comparison with Au nanofluid, and such a behavior was due to contribution of each photo-heated NP, evidencing that the TiN NPs based working fluid was not agglomerated in our experiments under solar illumination. The thermal efficiency of DASC using TiN nanofluid exhibited 80% better efficiency compared to that of spherical Au NPs. These results evidenced that TiN nanofluids can be a promising candidate for photothermal assisted applications. Therefore, the laser-synthesized TiN nanofluids can potentially present an ideal object for DASC due to its high performance, superior stability in the absence of ligands and cost efficient fabrication process.

CRediT authorship contribution statement

Sajid Farooq: Conceptualization, Data curation, Formal analysis, Software, Writing – original draft. **Caio V.P. Vital:** Methodology, Investigation, Formal analysis, Data curation, Conceptualization. **Gleb Tikhonowski:** Methodology, Investigation, Formal analysis. **Anton A. Popov:** Methodology, Investigation, Formal analysis, Data curation. **Sergey M. Klimentov:** Project administration, Methodology, Formal analysis, Data curation. **Luis A.G. Malagon:** Methodology, Investigation, Formal analysis, Conceptualization. **Renato E. de Araujo:** Writing

– review & editing, Validation, Project administration, Methodology, Formal analysis, Conceptualization. **Andrei V. Kabashin:** Conceptualization, Formal analysis, Methodology, Supervision, Writing – original draft, Writing – review & editing. **Diego Rativa:** Supervision, Project administration, Methodology, Formal analysis, Conceptualization.

Declaration of competing interest

The authors declare that they have no known competing financial interests or personal relationships that could have appeared to influence the work reported in this paper.

Data availability

Data will be made available on request.

Acknowledgment

G.T., A.A.P., S.M.K. and A.V.K. are grateful to the Ministry of Science and Education of the Russian Federation within the Agreement no. 075-15-2021-1347 for the infrastructure put at their disposal. A.A.P. acknowledges contribution of the Russian Science Foundation (Project 22-72-00015) for fabrication of and characterization of samples. Authors are grateful to Conselho Nacional de Desenvolvimento Científico e Tecnológico (CNPq), the National Institute of Science and Technology of Photonics (INCT de Fotônica), and the Coordenação de Aperfeiçoamento de Pessoal de Nível Superior (CAPES) for financial supports.

References

[1] N. Kannan, D. Vakeesan, Solar energy for future world: a review, Renew. Sustain. Energy Rev. 62 (2016) 1092–1105.
[2] S. Mekhilef, R. Saidur, A. Safari, A review on solar energy use in industries, Renew. Sustain. Energy Rev. 15 (2011) 1777–1790.
[3] H. Sharon, K. Reddy, A review of solar energy driven desalination technologies, Renew. Sustain. Energy Rev. 41 (2015) 1080–1118.
[4] G.K. Singh, Solar power generation by pv (photovoltaic) technology: a review, Energy 53 (2013) 1–13.
[5] M. Thirugnanasambandam, S. Iniyan, R. Goic, A review of solar thermal technologies, Renew. Sustain. Energy Rev. 14 (2010) 312–322.
[6] M. Potenza, M. Milanese, G. Colangelo, A. de Risi, Experimental in- vestigation of transparent parabolic trough collector based on gas-phase nanofluid, Appl. Energy 203 (2017) 560–570.
[7] Y. Tian, C.-Y. Zhao, A review of solar collectors and thermal energy storage in solar thermal applications, Appl. Energy 104 (2013) 538–553.
[8] X.-Q. Wang, A.S. Mujumdar, Heat transfer characteristics of nanofluids: a review, Int. J. Therm. Sci. 46 (2007) 1–19.
[9] P. Visconti, P. Primiceri, P. Costantini, G. Colangelo, G. Cavalera, Measurement and control system for thermosolar plant and performance comparison between traditional and nanofluid solar thermal collectors, Int. J. Smart Sens. Intell. Syst. 9 (2016).
[10] H. Tyagi, P. Phelan, R. Prasher, Predicted efficiency of a low-temperature nanofluid-based direct absorption solar collector, J. Sol. Energy Eng. 131 (2009), 041004.
[11] Z. Said, S. Arora, S. Farooq, L.S. Sundar, C. Li, A. Allouhi, Recent advances on improved optical, thermal, and radiative characteristics of plasmonic nanofluids: Academic insights and perspectives, Sol. Energy Mater. Sol. Cell. 236 (2022), 111504.
[12] X. Yang, Z.-h. Liu, A kind of nanofluid consisting of surface- functionalized nanoparticles, Nanoscale Res. Lett. 5 (2010) 1324–1328.
[13] S. Murshed, K. Leong, C. Yang, Enhanced thermal conductivity of tio2—water based nanofluids, Int. J. Therm. Sci. 44 (2005) 367–373.
[14] F. Iacobazzi, M. Milanese, G. Colangelo, M. Lomascolo, A. de Risi, An explanation of the al2o3 nanofluid thermal conductivity based on the phonon theory of liquid, Energy 116 (2016) 786–794.
[15] M. Milanese, F. Iacobazzi, G. Colangelo, A. de Risi, An investigation of layering phenomenon at the liquid–solid interface in cu and cuo based nanofluids, Int. J. Heat Mass Tran. 103 (2016) 564–571.
[16] S. Farooq, D. Rativa, Z. Said, R.E. de Araujo, High performance blended nanofluid based on gold nanorods chain for harvesting solar radiation, Appl. Therm. Eng. 218 (2023), 119212.
[17] H.-t. Zhu, Y.-s. Lin, Y.-s. Yin, A novel one-step chemical method for preparation of copper nanofluids, J. Colloid Interface Sci. 277 (2004) 100–103.
[18] C. Qin, K. Kang, I. Lee, B.J. Lee, Optimization of a direct absorption solar collector with blended plasmonic nanofluids, Sol. Energy 150 (2017) 512–520.
[19] H. Duan, R. Chen, Y. Zheng, C. Xu, Photothermal properties of plasmonic nanoshell-blended nanofluid for direct solar thermal absorption, Opt Express 26 (2018) 29956–29967.
[20] S. Farooq, C.V. Vital, L.A. Gómez-Malagón, R.E. de Araujo, D. Rativa, Thermo-optical performance of iron-doped gold nanoshells-based nanofluid on direct absorption solar collectors, Sol. Energy 208 (2020) 1181–1188.
[21] K. Suganthi, K. Rajan, Metal oxide nanofluids: review of formulation, thermo-physical properties, mechanisms, and heat transfer performance, Renew. Sustain. Energy Rev. 76 (2017) 226–255.
[22] M. Milanese, G. Colangelo, A. Cretì, M. Lomascolo, F. Iacobazzi, A. De Risi, Optical absorption measurements of oxide nanoparticles for application as nanofluid in direct absorption solar power systems– part i: water-based nanofluids behavior, Sol. Energy Mater. Sol. Cell. 147 (2016) 315–320.
[23] M. Milanese, G. Colangelo, A. Cretì, M. Lomascolo, F. Iacobazzi, A. De Risi, Optical absorption measurements of oxide nanoparticles for application as nanofluid in direct absorption solar power systems– part ii: zno, ceo2, fe2o3 nanoparticles behavior, Sol. Energy Mater. Sol. Cell. 147 (2016) 321–326.
[24] G.Z. y-la, J.P. Vallejo, L. Lugo, Isobaric heat capacity and density of ethylene glycol based nanofluids containing various nitride nanoparticle types: an experimental study, J. Mol. Liq. 261 (2018) 530–539.
[25] W. Chen, C. Zou, X. Li, Application of large-scale prepared mwcnts nanofluids in solar energy system as volumetric solar absorber, Sol. Energy Mater. Sol. Cell. 200 (2019), 109931.
[26] Z. Hong, J. Pei, Y. Wang, B. Cao, M. Mao, H. Liu, H. Jiang, Q. An, X. Liu, X. Hu, Characteristics of the direct absorption solar collectors based on reduced graphene oxide nanofluids in solar steam evaporation, Energy Convers. Manag. 199 (2019), 112019.
[27] X. Wang, Y. He, M. Chen, Y. Hu, Zno-au composite hierarchical parti- cles dispersed oil-based nanofluids for direct absorption solar collectors, Sol. Energy Mater. Sol. Cell. 179 (2018) 185–193.
[28] T. Yousefi, F. Veysi, E. Shojaeizadeh, S. Zinadini, An experimental investigation on the effect of al2o3–h2o nanofluid on the efficiency of flat-plate solar collectors, Renew. Energy 39 (2012) 293–298.
[29] G. Colangelo, M. Milanese, et al., Numerical simulation of thermal efficiency of an innovative al2o3 nanofluid solar thermal collector: influence of nanoparticles concentration, Therm. Sci. 21 (2017) 2769–2779.
[30] G. Colangelo, E. Favale, M. Milanese, G. Starace, A. De Risi, Experimental measurements of al 2 o 3 and cuo nanofluids interaction with microwaves, J. Energy Eng. 143 (2017), 04016045.
[31] F. Iacobazzi, M. Milanese, G. Colangelo, A. de Risi, A critical analysis of clustering phenomenon in al2o3 nanofluids, J. Therm. Anal. Calorim. 135 (2019) 371–377.
[32] S. Farooq, T.T. da Silva Correia, T.M. Yoshimura, S. de Toledo Pereira, M. S. Ribeiro, R.E. de Araujo, Methylene blue-mediated photoinactivation of staphylococcus aureus assisted by gold nanoshells, in: XXVI Brazilian Congress on Biomedical Engineering, Springer, 2019, pp. 841–845.
[33] A.R. Mallah, S.N. Kazi, M.N.M. Zubir, A. Badarudin, Blended morphologies of plasmonic nanofluids for direct absorption applications, Appl. Energy 229 (2018) 505–521.
[34] B. Lim, Y. Xia, Metal nanocrystals with highly branched morphologies, Angew. Chem. Int. Ed. 50 (2011) 76–85.
[35] P.K. Jain, K.S. Lee, I.H. El-Sayed, M.A. El-Sayed, Calculated absorption and scattering properties of gold nanoparticles of different size, shape, and composition: applications in biological imaging and biomedicine, J. Phys. Chem. B 110 (2006) 7238–7248.
[36] E.P. Bandarra Filho, O.S.H. Mendoza, C.L.L. Beicker, A. Menezes, D. Wen, Experimental investigation of a silver nanoparticle-based direct absorption solar thermal system, Energy Convers. Manag. 84 (2014) 261–267.
[37] M. Chen, Y. He, J. Zhu, D.R. Kim, Enhancement of photo-thermal conversion using gold nanofluids with different particle sizes, Energy Convers. Manag. 112 (2016) 21–30.
[38] D. Rativa, L.A. Gómez-Malagón, Solar radiation absorption of nanofluids containing metallic nanoellipsoids, Sol. Energy 118 (2015) 419–425.
[39] U. Guler, S. Suslov, A.V. Kildishev, A. Boltasseva, V.M. Shalaev, Colloidal plasmonic titanium nitride nanoparticles: properties and applications, Nanophotonics 4 (2015) 269–276.
[40] A. Lalisse, G. Tessier, J. Plain, G. Baffou, Plasmonic efficiencies of nanoparticles made of metal nitrides (tin, zrn) compared with gold, Sci. Rep. 6 (2016) 1–10.
[41] S. Ishii, R.P. Sugavaneshwar, T. Nagao, Titanium nitride nanoparticles as plasmonic solar heat transducers, J. Phys. Chem. C 120 (2016) 2343–2348.
[42] G.Z. y-la, J. Fal, P. Estellé, Thermophysical and dielectric profiles of ethylene glycol based titanium nitride (tin–eg) nanofluids with various size of particles, Int. J. Heat Mass Tran. 113 (2017) 1189–1199.
[43] L. Wang, G. Zhu, M. Wang, W. Yu, J. Zeng, X. Yu, H. Xie, Q. Li, Dual plasmonic au/tin nanofluids for efficient solar photothermal conversion, Sol. Energy 184 (2019) 240–248.
[44] X. Yang, C. Li, L. Yang, Y. Yan, Y. Qian, Reduction-nitridation synthesis of titanium nitride nanocrystals, J. Am. Ceram. Soc. 86 (2003) 206–208.
[45] H. Zhang, F. Li, Q. Jia, Preparation of titanium nitride ultrafine pow- ders by sol–gel and microwave carbothermal reduction nitridation methods, Ceram. Int. 35 (2009) 1071–1075.
[46] J. Tavares, S. Coulombe, J. Meunier, Synthesis of cubic-structured monocrystalline titanium nitride nanoparticles by means of a dual plasma process, J. Phys. Appl. Phys. 42 (2009), 102001.
[47] O. Abdulmunem, K. Hassoon, M. Gaafar, A. Rahimi-Iman, J.C. Balzer, Tin nanoparticles for enhanced thz generation in tds systems, J. Infrared, Millim. Terahertz Waves 38 (2017) 1206–1214.

[48] Y. Zhang, L. Liu, K. Li, D. Hou, J. Wang, Enhancement of energy utilization using nanofluid in solar powered membrane distillation, Chemosphere 212 (2018) 554–562.
[49] W. He, K. Ai, C. Jiang, Y. Li, X. Song, L. Lu, Plasmonic titanium nitride nanoparticles for in vivo photoacoustic tomography imaging and photothermal cancer therapy, Biomaterials 132 (2017) 37–47.
[50] A. Fojtik, A. Henglein, Laser ablation of films and suspended particles in a solvent: formation of cluster and colloid solutions, Ber. Bunsen Ges. 97 (1993) 252–254.
[51] M.S. Sibbald, G. Chumanov, T.M. Cotton, Reduction of cytochrome c by halide-modified, laser-ablated silver colloids, J. Phys. Chem. A 100 (1996) 4672–4678.
[52] A.V. Kabashin, M. Meunier, Synthesis of colloidal nanoparticles during femtosecond laser ablation of gold in water, J. Appl. Phys. 94 (2003) 7941–7943.
[53] K. Maximova, A. Aristov, M. Sentis, A.V. Kabashin, Size-controllable synthesis of bare gold nanoparticles by femtosecond laser fragmentation in water, Nanotechnology 26 (2015), 065601.
[54] A.A. Popov, G. Tselikov, N. Dumas, C. Berard, K. Metwally, N. Jones, A. Al-Kattan, B. Larrat, D. Braguer, S. Mensah, et al., Laser- synthesized tin nanoparticles as promising plasmonic alternative for biomedical applications, Sci. Rep. 9 (2019) 1194.
[55] T. Baati, A. Al-Kattan, M.-A. Esteve, L. Njim, Y. Ryabchikov, F. Chaspoul, M. Hammami, M. Sentis, A.V. Kabashin, D. Braguer, Ultrapure laser-synthesized si-based nanomaterials for biomedical applications: in vivo assessment of safety and biodistribution, Sci. Rep. 6 (2016) 1–13.
[56] A.V. Kabashin, V.Y. Timoshenko, What theranostic applications could ultrapure laser-synthesized si nanoparticles have in cancer?, 2016.
[57] A.V. Kabashin, A. Singh, M.T. Swihart, I.N. Zavestovskaya, P.N. Prasad, Laser-processed nanosilicon: a multifunctional nanomaterial for energy and healthcare, ACS Nano 13 (2019) 9841–9867.
[58] S. Reichenberger, G. Marzun, M. Muhler, S. Barcikowski, Perspective of surfactant-free colloidal nanoparticles in heterogeneous catalysis, ChemCatChem 11 (2019) 4489–4518.
[59] S. Hebié, Y. Holade, K. Maximova, M. Sentis, P. Delaporte, K.B. Kokoh, T. W. Napporn, A.V. Kabashin, Advanced electrocatalysts on the basis of bare au nanomaterials for biofuel cell applications, ACS Catal. 5 (2015) 6489–6496.
[60] J.-P. Sylvestre, S. Poulin, A.V. Kabashin, E. Sacher, M. Meunier, J.H. Luong, Surface chemistry of gold nanoparticles produced by laser abla- tion in aqueous media, J. Phys. Chem. B 108 (2004) 16864–16869.
[61] M.E.S. Jendrzej, B. Gokce, S. Barcikowski, How size determines the value of gold: economic aspects of wet chemical and laser-based metal colloid synthesis, ChemPhysChem 18 (2017) 1012–1019.
[62] U. Guler, J.C. Ndukaife, G.V. Naik, A.A. Nnanna, A.V. Kildishev, V.M. Shalaev, A. Boltasseva, Local heating with lithographically fabricated plasmonic titanium nitride nanoparticles, Nano Lett. 13 (2013) 6078–6083.
[63] G. Baffou, Thermoplasmonics, World Scientific, 2017.
[64] K. Jiang, D.A. Smith, A. Pinchuk, Size-dependent photothermal conversion efficiencies of plasmonically heated gold nanoparticles, J. Phys. Chem. C 117 (2013) 27073–27080.
[65] D. Rativa, L.A. Gómez-Malagón, Colloidal plasmonic structures for harvesting solar radiation, Renew. Energy 118 (2018) 947–954.
[66] M. Chen, Y. He, J. Zhu, D. Wen, Investigating the collector efficiency of silver nanofluids based direct absorption solar collectors, Appl. Energy 181 (2016) 65–74.
[67] R. Saidur, T. Meng, Z. Said, M. Hasanuzzaman, A. Kamyar, Evaluation of the effect of nanofluid-based absorbers on direct solar collector, Int. J. Heat Mass Tran. 55 (2012) 5899–5907.
[68] M. Chen, Y. He, X. Wang, Y. Hu, Complementary enhanced solar thermal conversion performance of core-shell nanoparticles, Appl. Energy 211 (2018) 735–742.
[69] J. Zeng, Y. Xuan, Enhanced solar thermal conversion and thermal conduction of mwcnt-sio2/ag binary nanofluids, Appl. Energy 212 (2018) 809–819.
[70] Y. Xuan, H. Duan, Q. Li, Enhancement of solar energy absorption using a plasmonic nanofluid based on tio 2/ag composite nanoparticles, RSC Adv. 4 (2014) 16206–16213.
[71] F.E.B. Bioucas, M.H. Rausch, J. Schmidt, A. Bück, T.M. Koller, A.P. Fröba, Effective thermal conductivity of nanofluids: measurement and prediction, Int. J. Thermophys. 41 (2020) 1–27.
[72] R. Streubel, S. Barcikowski, B. Gökce, Continuous multigram nanoparticle synthesis by high-power, high-repetition-rate ultrafast laser ablation in liquids, Opt. Lett. 41 (2016) 1486–1489.